Sánchez Tovar, R.; Montañés Sanjuan, MT.; García Antón, J.; Guenbour, A.; Ben Bachir, A. (2011). Corrosion behaviour of micro-plasma arc welded stainless steels in H3PO4 under flowing conditions at different temperatures. Corrosion Science. 53(4):1237-1246. doi:10.1016/j.corsci.2010.12.017.

Corrosion behaviour of micro-plasma arc welded stainless steels in H_3PO_4 under flowing conditions at different temperatures

R. Sánchez-Tovar[a], M.T. Montañés[a], J. García-Antón[a*], A. Guenbour[b], A. Ben-Bachir[b]

[a] Ingeniería Electroquímica y Corrosión (IEC). Departamento de Ingeniería Química y Nuclear. Universidad Politécnica de Valencia, 46022, Spain. [*]jgarciaa@iqn.upv.es

[b] Laboratoire de Corrosion-Electrochimie, Faculté des Sciences, Université Mohammed V- Agdal, BP 1014 Rabat, Morocco

Abstract

This paper studies the general corrosion behaviour of the micro-plasma arc welded AISI 316L stainless steel in phosphoric acid at different temperatures (25 to 60 ºC) and at a Reynolds number of 1456. Galvanic corrosion has been studied using zero resistance ammeter (ZRA) measurements and polarization curves (by the mixed potential theory). Results show that the microstructure of the stainless steel is modified due to the micro-plasma arc welding procedure. Coupled current density values obtained from polarization curves increase with temperature. ZRA tests present the highest i_G values at 60 ºC; however, the values are very close to zero for all the temperatures studied. This is in agreement with the low value of the compatibility limit and of the parameter which evaluates the importance of the galvanic phenomenon. Both techniques present the most positive potentials at the highest temperature. This study reveals that micro-plasma arc welded AISI 316L stainless steels are appropriated working in the studied H_3PO_4 media from a corrosion point of view for all the temperatures analysed.

Keywords: A. Acid solutions; A. Stainless steel; B. Polarization; C. Welding

1. Introduction

Austenitic stainless steels, as well as their welded forms, are widely used in the phosphoric acid industry, for instance, in piping systems. This is due to the fact that they have excellent corrosion and heat resistance with good mechanical properties over a wide range of temperatures [1]. In particular, AISI 316L stainless steel (SS) is used for its good mechanical properties and corrosion resistance [2]. Therefore, AISI 316L SS is suitable to store and transport phosphoric acid at different temperatures. In particular, when high temperature treatments are applied, such as welding processes, corrosion along the grain boundaries could take place [3]. However, AISI 316L stainless steels are appropriate owing to their low carbon content. Welding introduces metallurgical changes and residual stresses in materials, diminishing their corrosion resistance. In fact, welds are recognized as zones that are particularly sensitive to corrosion [4]. Furthermore, the use of welded materials could result in the formation of galvanic pairs that may accelerate the corrosion processes and temperature can enhance these corrosion problems [5, 6]. On the other hand, the effect of fluid flow has been considered as one of the major problems in the corrosion field since it can also increase corrosion rates [7].

Plasma arc welding (PAW) is an innovative arc welding process [8] similar to gas tungsten arc welding (GTAW). The key difference from GTAW is that in PAW the plasma arc can be separated from the shielding gas envelope. PAW represents an advance over GTAW due to its greater energy concentration, deep and narrow penetration achievement and greater arc stability. Micro-plasma arc welding (MPAW) is a variation of the PAW process and uses intensities lower than 15 A. Several authors have studied the MPAW technology [9-12]. However, there is no research related to micro-plasma arc

welded AISI 316L stainless steels that takes into consideration galvanic corrosion, especially in phosphoric acid solutions.

The use of polarization curves has become widespread during the last years due to its versatility [13]. However, the application of a zero-resistance ammeter (ZRA) as an electrochemical measurement technique is gaining importance because it does not disturb the system under investigation. ZRA can record the potential and current fluctuations in the corroding electrodes during a corrosion process [14].

Many studies have focused on the influence of temperature on corrosion in phosphoric acid, such as corrosion of steel at different acid concentrations [15], corrosion behaviour of stainless steels in H_3PO_4 polluted by sulphide ions [16] and corrosion behaviour of graphite and stainless steel in polluted phosphoric acid [17]. However, these studies are based on weight loss and polarization curves measurements. Galvanic corrosion is one of the most common and damaging forms of corrosion. Hence, controlling galvanic corrosion is of great economic importance in many industries [18]. This work focuses on the real corrosion behaviour of a welded pipeline. The galvanic corrosion generated between a micro-plasma arc welded alloy and the rest of the non-welded pipeline, which carries a phosphoric acid solution, has been studied. The weldment consists of the weld bead and the heat affected zone (HAZ). Several works have studied the corrosion behaviour of welded materials as a composite specimen; that is, the welded material includes the weld metal and the HAZ [19-24] and in some cases, the base material [25]. Furthermore, the galvanic corrosion of non-welded/welded stainless steels (the latter as a composite specimen: including the weld metal and the HAZ) has been studied by means of ZRA measurements [26] and polarization curves [27]. The objective of this work is to

study the effect of temperature on the galvanic corrosion of the non-welded/micro-plasma arc welded AISI 316L SS pair at a Reynolds number (*Re*) of 1456 by means of polarization curves (according to the mixed potential theory, MPT [28]) and ZRA measurements. The effect of the innovative MPAW technique on the general corrosion behaviour of the materials in H_3PO_4 media will be analysed. The corrosion process of a non-welded SS will be compared to the MPA welded alloy one. Furthermore, the consequences of having a pipeline with a MPA welded material in electrical contact with a non-welded one will be also analysed.

2. Experimental

2.1. Materials

2.1.1. Corrosion studies

The materials studied were tubes 14 mm and 16 mm in inner and external diameter, respectively, and 20 mm in length (an area of 8.8 cm^2 was exposed to the solution). They were made of AISI 316L SS (16.957 wt. % Cr, 10.171 wt. % Ni, 1.337 wt. % Mn, 2.298 wt. % Mo, 0.004 wt. % S, 0.368 wt. % Si, 0.030 wt. % P, 0.022 wt. % C, Bal. wt. % Fe) and micro-plasma arc welded AISI 316L SS. The base material was always AISI 316L SS and it was welded with AISI 316L filler alloy (18.160 wt. % Cr, 12.100 wt. % Ni, 1.860 wt. % Mn, 2.540 wt. % Mo, 0.007 wt. % S, 0.760 wt. % Si, 0.018 wt. % P, 0.010 wt. % C, 0.080 wt. % Cu, 0.050 wt. % N, Bal. wt. % Fe) and with backing gas (99.9% Ar). Two tubes (10 mm in length) were welded in order to obtain samples with the same size as the non-welded SS ones and to achieve a micro-plasma arc welded alloy composed mainly by the weld metal and the HAZ. The composition of the filler alloy is more noble than that of the base material. In spite of this, the compositions of both the base and the filler alloy are very similar in order to avoid future galvanic problems. The

argon backing gas was used to protect the inner surface of the materials during welding [29]. The flow rate of this shielding gas was 2.5 L/min. The welding process was carried out in two steps (step one: current = 11.3 A, voltage = 20 V, welding speed = 2.6 mm/s and step two: current = 13 A, voltage = 20 V, welding speed = 2.6 mm/s). The flow rate of the plasma gas was 6.5 L/min. Figure 1 shows in a scheme the materials used in this work, as well as, a photograph of the non-welded and the micro-plasma arc welded AISI 316L SS tubes. Figure 2 shows a photograph of the inner surface of the tubes. This figure also shows the differences between the non-welded (base material) and the micro-plasma arc welded alloy (i.e. the weld bead and the HAZ).

2.1.2. Analysis of the microstructure

To estimate the possible variations in the microstructure produced due to the MPAW procedure, each material (non-welded and the MPA welded alloy) was cut lengthwise and covered in cold mounting acrylic resin (DuroFix-2, Struers) for the embedding of specimens. Then, the samples were wet abraded from 220 silicon carbide (SiC) grit to 4000 SiC grit (in several steps; i.e. 220, 500, 1000, 2500 and 4000). Then, the mounted samples were polished with 1 and 0.3 micron alumina and were rinsed with distilled water, followed by ethanol. Once the samples were polished, metallographic etching was carried out according to ASM International [30]. The etchant composition consisted of 10 mL of nitric acid (65 wt. %), 10 mL of acetic acid (99-100 wt. %), 15 mL of hydrochloric acid (37-38 wt. %) and 5 mL of glycerine (100 wt. %). Samples were immersed in the etching solution during 90 seconds and then rinsed with distilled water, followed by ethanol. Afterwards, materials were examined by light microscopy (LM) and scanning electron microscopy (SEM) to reveal their microstructure and compare it with the microstructure of the base alloy.

2.2. Hydrodynamic circuit

A hydrodynamic circuit, based on a circuit designed in a previous work [31], was used to study corrosion under flowing conditions. It consists of a centrifugal pump, a flow-meter, a thermostat to regulate the solution temperature, a test section (where the tubes are assessed), a valve to drain the system and several glass devices: for the reference electrode (Ag/AgCl, 3M KCl), for the auxiliary electrode (Pt), for the gas output, to introduce the solution into the flow circuit and to bubble an inert gas. Medical grade silicone flexible tubes were used to assemble the different elements. Fully developed flow was assured using a 90-cm-long Teflon rigid tube of the same inner diameter as the test tubes upstream of the test section.

2.3. Operating conditions

Materials were tested in a 5.5 M H_3PO_4 solution (40 wt. % H_3PO_4) made with deionised water. The experiments were carried out at a Reynolds number of 1456 at 25, 40 and 60 ^oC in order to study the influence of temperature on galvanic corrosion under flowing conditions. These concentration and temperature conditions are typical in the phosphoric acid industry [5].

2.4. Electrochemical tests

Two different electrochemical techniques were used in the corrosion studies: polarization curves and zero-resistance ammeter measurements. To perform the tests a potentiostat (Solartron 1285 provided with the Corrware software) was used.

Before each test, the tubes were degreased with ethanol and dried with air at room temperature. Nitrogen (99.99 %) was bubbled for 60 minutes prior the tests. All the tests were repeated at least three times in order to verify reproducibility.

2.4.1. Polarization curves

Before obtaining the cyclic potentiodynamic curves, the open circuit potential (*OCP*) was recorded for one hour. After the *OCP* test, the potential was reduced progressively to -400 $mV_{Ag/AgCl}$ (the potential was not reduce to more negative values in order to minimise the formation of hydrogen). Then, the working electrode potential was scanned from -400 $mV_{Ag/AgCl}$ to the anodic direction until the current density reached 0.2 mA/cm^2, using a scan rate of 1 mV/s. These operating conditions were defined for the H_3PO_4 system in order to obtain polarization curves for the determination of corrosion parameters. Figure 3 shows a schematic diagram of the physical arrangement of the electrodes in the test section.

The galvanic corrosion between the non-welded AISI 316L SS and the micro-plasma arc welded AISI 316L SS was evaluated from the polarization curves, by superimposing the potentiodynamic curves of both materials. The predicted coupled potential (E_{coup}) and the coupled current density (i_{coup}) of the pair were estimated from the intersection point of the anodic curve of one alloy with the cathodic curve of the other one, according to the mixed potential theory [28]. The mixed potential theory has been widely used to study galvanic corrosion [32-35] and, in particular, the galvanic corrosion behaviour of non-welded/welded couples [36-40].

2.4.2. Zero-resistance ammeter (ZRA) measurements

The galvanic current density (i_G) and the galvanic potential (E_G) established between the pair were measured with a ZRA every 0.5 s for 8 h. The tests were designed with the non-

welded AISI 316L SS as working electrode (WE) and the micro-plasma arc welded AISI 316L SS grounded. Figure 4 shows a schematic diagram of the physical arrangement of the electrodes in the test section. The tubes were insulated by a Teflon intermediate assembly piece which was 14 mm in inner diameter, as well as the inner diameter of the tubes. The current sign was positive when the electrons flowed from working electrode; thus, non-welded AISI 316L SS was corroding. Current values were negative when the electrons flowed in the opposite direction, that is, the micro-plasma arc welded AISI 316L SS was corroding.

3. Results and discussion

3.1. Effect of MPAW on AISI 316L SS microstructure

To analyse the effect of welding on the microstructure of the AISI 316L SS a microstructural analysis of the materials cut lengthwise and covered in resin was performed by means of light microscopy and scanning electron microscopy. Figure 5a shows the microstructure of the non-welded AISI 316L SS after etching. The microstructure presents equiaxed grains in an austenitic single-phase. As shown in Figure 5b, the microstructure of the HAZ in the micro-plasma arc welded alloy exhibits an austenitic microstructure. The microstructure of this zone is also characterised by an increase in grain size [41, 42]. On the other hand, Figure 5c shows the microstructure of the weld zone corresponding to the micro-plasma arc welded AISI 316L SS. The weld zone has columnar grains where delta-ferrite can be found [43]. All these facts indicate that the microstructure of the AISI 316L SS is modified as a consequence of the MPAW process.

3.2. Effect of MPAW on AISI 316L corrosion behaviour

Figure 6 shows the open circuit potential registers corresponding to the non-welded AISI 316L SS (Figure 6a) and to the micro-plasma arc welded AISI 316L SS (Figure 6b) at the different temperatures analysed. Open circuit potentials shift towards more positive values and seem to stabilise with time, indicating that non-welded and micro-plasma arc welded AISI 316L SS have a passive behaviour in phosphoric acid at the different temperatures studied.

Concretely chromium oxide is considered the main passive component of the passive film in the anodic polarization of stainless steels. On the other hand, phosphoric acid media favour the formation of iron phosphates [44]. Phosphate species can precipitate with dissolved iron species to form iron phosphates, since these compounds are characterised by a low solubility. Precipitation of iron phosphate occurs at the interface [45]; that is:

$$6H_3PO_4 + 3Fe \rightarrow 3Fe(H_2PO_4)_2 + 3H_2$$

$$3Fe(H_2PO_4)_2 \rightarrow Fe_3(PO_4)_2 + 4H_3PO_4$$

In phosphoric acid solutions, due to the low oxidative capacity of the stainless steel surface [46], a predominant formation of a soluble $Fe(H_2PO_4)_2$ phosphate compound might occur on stainless steel which can result in the formation of a porous film.

The open circuit potential values (*OCP*) were obtained as the arithmetic mean of the last five minute values of open circuit potential measurements [47]: 160 ± 15, 185 ± 20 and 198 ± 17 $mV_{Ag/AgCl}$ at 25, 40 and 60 ºC for the non-welded AISI 316L SS and -132 ± 20, 154 ± 12 and 195 ± 27 $mV_{Ag/AgCl}$ at 25, 40 and 60 ºC for the micro-plasma arc welded AISI 316L SS, respectively. The *OCP* values of the non-welded AISI 316L SS are more positive than those corresponding to the micro-plasma arc welded stainless

steels, whereas these differences diminish with temperature; at 60 ºC the *OCP* values are almost the same (198 and 195 $mV_{Ag/AgCl}$ for the non-welded and the micro-plasma arc welded AISI 316L SS, respectively).

Figure 7 shows the cyclic potentiodynamic curves obtained for the non-welded and the micro-plasma arc welded AISI 316L SS, which are typical of passive materials. Since tests were reproducible, Figure 7 shows just one of the curves obtained for each temperature. The *OCP* mean values of the materials (indicated in the previous paragraph) are represented by vertical lines in Figure 7. The curves presented in Figure 7a (non-welded SS) show an active region, a transition peak from the active to the passive state, a wide passive range and a further current increase above the passive region. This is in agreement with the potentiodynamic curves registered by Rodríguez [48] in acidic solutions. The registers shown in Figure 7b (micro-plasma arc welded SS) do not present the transition peak. The active-passive transition on the anodic branch is related to better passive properties of the film formed [13, 49]. The *OCP* values obtained at the different temperatures indicate that the non-welded and, at 40 and 60 ºC, the micro-plasma arc welded AISI 316L SS passivate spontaneously, as the *OCP* values correspond to the passive range of stainless steels. On the other hand, the *OCP* value of the micro-plasma arc welded material at 25 ºC is situated on the active region of the polarization curve.

Table 1 shows the mean values of the corrosion potentials (E_{corr}) and corrosion current densities (i_{corr}) obtained from polarization curves. Table 1 shows that corrosion current densities of the non-welded AISI 316L SS are higher than those obtained for the micro-plasma arc welded materials, especially as temperature increases. This could be due to the higher Cr, Ni and Mo contents of the materials welded with filler alloy. In fact, the

role of Ni and Mo in stainless steels at anodic potentials in acid solutions is to stabilise the passive film and to eliminate the active surface sites [17]. Moreover, nitrogen content of the filler alloy, in presence of Mo, generally improves corrosion resistance [50]. On the other hand, corrosion potentials are more active (more negative) for the non-welded stainless steels. Furthermore, corrosion potential values determined from the polarization curves are more active than *OCP* ones, especially for the non-welded AISI 316L SS; this is due to the applied polarization [51, 52].

Table 2 shows the mean values of the critical potentials (E_c) and passivation current densities (i_p) obtained from the anodic branch of polarization curves. The potential at which the current density reaches 100 $\mu A/cm^2$ was reported as E_c [53]. Passivation current densities were obtained as the mean value between the lowest current density after the transition peak from the active to the passive state until the current density values start to increase drastically with an increase in potential. Table 2 shows that critical potentials are of the same magnitude order for the non-welded and the micro-plasma arc welded materials. On the other hand, Table 2 also shows that welding modifies the characteristics of the materials increasing the passivation current density. However, this difference is lower as temperature increases.

Figure 8 represents the difference between E_c and E_{corr} (passivity range) obtained from their mean values. This difference is used as a measure of passivity of the materials. The greater the difference, the wider the range of potentials in which the alloys remain passive. Figure 8 shows that passivity ranges are larger for the non-welded AISI 316L SS (Figure 7a). This is due to the fact that while critical potential values are of the same magnitude order, corrosion potentials for the non-welded materials are more negative

than for the micro-plasma arc welded alloys. This issue, together with the lower passivation current densities obtained for the non-welded alloy, results in better passivation film properties of the non-welded stainless steels. This is in agreement with the active-passive transition peak shown in Figure 9a for the non-welded materials.

3.3. Influence of temperature on corrosion of the uncoupled materials

As illustrated in Figure 6, the most negative *OCP* values are obtained at 25 ºC. Thus, it can be expected that temperature enhances not only the kinetics of the corrosion reaction [5, 6], but also the kinetics of the passivation one.

Table 1 shows that temperature increases corrosion current densities of the non-welded AISI 316L SS, since it enhances the corrosion rate. However, for the micro-plasma arc welded materials the trend is different. That is, the corrosion current density diminishes from 25 to 40 and at 60 ºC it remains almost constant. This could be due to the higher Cr, Ni and Mo contents of the materials welded with filler alloy. On the other hand, corrosion potentials shift to more positive values when temperature changes from 25 to 40 ºC. Furthermore, from 40 to 60 ºC corrosion potential values seem to remain constant, especially for the non-welded AISI 316L SS. This tendency towards more positive values was also observed for the *OCP* of the materials in Figure 6.

Table 2 shows that temperature shifts critical potentials to more active values, both for the non-welded and the micro-plasma arc welded stainless steels. The critical potential indicates the breakdown of the passive film [54] and temperature provokes that this breakdown occurs at more negative potentials. On the other hand, Table 2 also shows a slightly increase in the passivation current densities as temperature increases for the non-

welded AISI 316L SS, while the effect of temperature on the passivation current density of the micro-plasma arc welded material is the opposite, as it occurs with corrosion current densities. This could be due to temperature may have a passive effect on micro-plasma arc welded AISI 316L SS. On the other hand, temperature seems to decrease the passivity ranges of the non-welded and micro-plasma arc welded SS, especially from 25 to 40 ºC (Figure 8). Thus, in spite of the fact that passivation current densities diminish with temperature for the micro-plasma arc welded alloy (Table 2), the passivity ranges decrease with temperature too. These opposite phenomena result in slight passivant effect of temperature.

3.4. Influence of temperature on the galvanic corrosion of the non-welded/micro-plasma arc welded materials obtained by ZRA measurements

Up to now, the corrosion behaviour of non-welded and micro-plasma arc welded AISI 316L SS in H_3PO_4 has been studied independently. However, in phosphoric acid industries, there is an electrical contact between both materials; therefore, galvanic corrosion might take place. This galvanic corrosion between the non-welded and the micro-plasma arc welded alloys at different temperatures was evaluated by means of the ZRA technique.

Figure 9 shows the galvanic current density (i_G) and the galvanic potential (E_G) profiles obtained during 8 h (since tests showed that i_G data were almost stable from the sixth hour) for the non-welded/micro-plasma arc welded AISI 316L SS pair in H_3PO_4 at a *Re* of 1456 and at all the temperatures studied by means of ZRA measurements. Since tests were reproducible, Figure 9 shows just one of the profiles obtained for each temperature.

Figure 9 shows that galvanic current densities are negative during the first hours of the tests; in particular, during the first hour, the first two hours and the first three hours of the tests carried out at 60, 40 and 25 ºC, respectively. Therefore, during these first hours, the anode of the pair is the micro-plasma arc welded AISI 316L SS. The general tendency of the galvanic current density in absolute value is to decrease with time (that is; the values tend to zero). This trend is favoured by temperature. This issue could be due to the fact that, in general, temperature enhances corrosion rates [5, 6]; consequently, passivation of the micro-plasma arc welded AISI 316L SS occurs earlier. Therefore, the drastic switch at 60 ºC might be due to temperature. Once passivation of the micro-plasma arc welded material takes place, there is a change in the polarity at the higher temperatures analysed, which means that the non-welded AISI 316L SS is corroding. At 40 ºC i_G values remain positive but near zero and at 60 ºC, galvanic current density tends to decrease with time and beyond the sixth hour, to stabilise. The decrease in galvanic current density is attributed to metal passivation due to the formation of a film which grows with time [55]. On the other hand, at 25 ºC galvanic current density values change to positive values during the fourth hour; later, i_G becomes negative but remains practically equal to zero.

The general tendency of the galvanic potential profiles is to become more positive with time. Therefore, the galvanic potential profile may represent the passivation phenomenon. Furthermore, the values seem to stabilise from the sixth hour of the tests; beyond that time, galvanic current density profiles become stable too at all the studied temperatures. The most noble galvanic potential corresponds to the highest temperature studied (60 ºC) and the most active to the lowest one (25 ºC).

Figure 9 also shows that the galvanic current density and the galvanic potential profiles have very few individual events; this is a characteristic of uniform corrosion processes [56]. Moreover, the most remarkable characteristic of uniform corrosion processes is to present low-amplitude potential and current signals [14], like those registered by the non-welded/micro-plasma arc welded AISI 316L SS pair.

Table 3 shows the mean values of the galvanic potentials and the galvanic current densities at the different temperatures studied for each hour of the test. As it can be observed, the i_G values are very low. Furthermore, galvanic potentials shift to more positive values with time. Therefore, passivity of the materials is expected in H_3PO_4 solutions.

3.5. Influence of temperature on the galvanic corrosion of the non-welded/micro-plasma arc welded materials obtained by the Mixed Potential Theory

Figure 10 shows the superimposing of the cyclic polarization curves of the non-welded/ micro-plasma arc welded AISI 316L SS galvanic pair, the predicted coupled potential (E_{coup}) and the coupled current density (i_{coup}) at the different temperatures studied. The shaded box shows the maximum and minimum values of the galvanic current density and the galvanic potential measured by the ZRA technique from the time that it was clearly distinguished that either the non-welded or the micro-plasma arc welded AISI 316L SS corrodes. The open circuit potential (*OCP*) values of the materials are represented by vertical lines. The ZRA and *OCP* data have been included in Figure 10 in order to compare later the techniques studied (open circuit and imposed potential measurements).

Figure 10 shows that in all the cases, the corrosion potential of the non-welded AISI 316L SS is more active than that obtained for the micro-plasma arc welded materials; therefore, polarization curves indicate that the non-welded AISI 316L SS is the anode of the pair at all the temperatures analysed; therefore, it will corrode while the micro-plasma arc welded material remains protected. This fact could be due to the higher Cr, Ni and Mo contents of the materials welded with filler alloy. Lee et al. [27] studied the corrosion behaviour of stainless steels using the flux-cored arc welding procedure. They observed that all the welded metals analysed (where the weld metal, fusion line and HAZ zone were contained) were the cathode of the pair when coupled with the base metal.

Table 4 shows the mean values of the predicted coupled potential and the coupled current density values obtained according to the mixed potential theory [28], as well as the differences between corrosion potentials of the cathodic and the anodic member of the pair (E_{corr_C} - E_{corr_A}) calculated from the mean values of the corrosion potentials and the i_{coup}/i_{corr} ratio, where i_{corr} is the mean value of the corrosion current density of the uncoupled anodic member and i_{coup} is the mean value of the coupled current density of the pair.

Similarly to the corresponding potentials of the uncoupled non-welded material, Table 4 shows that predicted coupled potentials have the same tendency to shift to more noble values as temperature increases. Minimal differences of 100-130 mV between the corrosion potential of the cathode and the anode of the pair (E_{corr_C} - E_{corr_A}) are necessary to consider the galvanic effect significant [57]. Table 4 shows that, at all the temperatures studied, the (E_{corr_C} - E_{corr_A}) values are lower than or close to 130 mV; therefore, the

galvanic effect on the non-welded/micro-plasma arc welded AISI 316L SS pair seems not to be significant.

On the other hand, coupled current densities of the pair increase with temperature, as it happened with the uncoupled non-welded AISI 316L SS. According to Mansfeld and Kendel [58], the relative increase in the corrosion rate of the anode of the galvanic pair could be expressed by the ratio i_{coup}/i_{corr}, where i_{corr} is the corrosion current density of the uncoupled anode. The magnitude of this ratio may be used as a guide to reflect the severity of the galvanic effect, and it was suggested that an i_{coup}/i_{corr} value lower than 5 implies compatibility of the members in a galvanic pair [59]. Table 4 shows that the i_{coup}/i_{corr} values are lower than 1.5 in all the cases analysed; therefore, it can be concluded that the galvanic corrosion of the non-welded/micro-plasma arc welded AISI 316L SS pair in a 5.5 M H_3PO_4 solution will not be severe.

In general, temperature increases the rate of most reactions following Arrhenius equation [60]. In the case of electrochemical reactions, temperature can favour the kinetics of corrosion reactions and, more specifically, the anodic dissolution of the metal [61-63]. The activation energy of the corrosion process can be obtained from Arrhenius-type plots according to the following equation:

$$i_{corr} = A\exp\left(-\frac{E_a}{RT}\right) \quad (1)$$

where E_a is the molar activation energy of the process (J/mol), R is the universal gas constant (8.314 J/(mol K)), T is the temperature (K) and A is a constant. Using the logarithm of the Arrhenius equation the following expression is obtained:

$$\log(i_{corr}) = \log(A) - \frac{E_a}{2.303RT} \quad (2)$$

Therefore, the activation energy values of a corrosion process can be determined from the slope of $\log(i_{corr})$ versus $1/T$ plots [64]. The molar activation energy of an electrochemical process refers to the energy level that must be overcome by one electron in the exchange through the electrode/electrolyte interphase. In this way, low E_a values indicate high corrosion rates. Moreover, the Arrhenius equation indicates that the greater the dependence of the corrosion rate on temperature, the higher the E_a values [65].

Corrosion current density values of the non-welded AISI 316L SS (Table 1), as well as the coupled current densities of the pair (Table 4), have been plotted according to Equation 2 in Figure 11. Figure 11 shows the linear plots encountered for the uncoupled and coupled non-welded AISI 316L SS. As it can be observed in Figure 11, both the experimental mean values of the corrosion current density of the non-welded AISI 316L SS and of the coupled current density of the pair fit well the Arrhenius plot. Furthermore, the E_a value obtained for the uncoupled non-welded AISI 316L SS (17.24 kJ/mol) is higher than that calculated from the mixed potential theory (MPT) for the galvanic pair (16.23 kJ/mol). This issue could be explained due to the fact that corrosion rate increases owing to the galvanic effect.

3.6. Polarization curves vs ZRA measurements

Figure 10 shows the comparison between the results obtained by means of the mixed potential theory and the ZRA technique under all the studied temperatures. According to the ZRA measurements, the black broken lines in Figure 10a indicate that the micro-plasma arc welded AISI 316L SS is corroding while the grey broken lines in Figures 10b

and 10c indicate that the non-welded alloy is the anode of the pair (in accordance with the sign criteria indicated in the section 2.4.2. of the Experimental).

Figure 10 shows that the galvanic potential values obtained by means of the ZRA technique are closer to the open circuit potential values (*OCP*) of the uncoupled materials rather than to the predicted coupled potentials (E_{coup}). Furthermore, the same tendency is observed for *OCP* values (Figure 6) and the galvanic potentials (Figure 9b); that is, E_G values shift to more positive values with time and stabilised.

The results show that the imposed potential measurements provide more active predicted coupled potentials and higher coupled current densities than those obtained using ZRA measurements. This could be explained due to the formation of a passive film during the open circuit tests, whereas this passive film is modified at the beginning of the polarization measurements owing to the applied potential [51, 52]. Coupled current density values obtained from the polarization curves increase with temperature. Regarding the ZRA tests, the highest i_G has been obtained at 60 ºC; however, the i_G values are very close to zero for all the temperatures studied. This is in agreement with the (E_{corr_C} - E_{corr_A}) values obtained (which are low or close to the minimum value necessary to consider the galvanic phenomenon significant), together with the low i_{coup}/i_{corr} values (in all the cases lower than 5). Hence, owing to these facts, micro-plasma arc welded AISI 316L stainless steels are appropriated working in the studied H_3PO_4 media from a corrosion point of view for all the temperatures analysed.

4. Conclusions

This work studies the general corrosion behaviour of AISI 316L stainless steels welded by means of the innovative micro-plasma arc welding technique. Additionally, this work also analyses the effect of temperature on the galvanic corrosion of the non-welded/micro-plasma arc welded AISI 316L SS pair in H_3PO_4 at a *Re* of 1456 using polarization curves and ZRA tests. The main conclusions are presented below.

1. The microstructure of AISI 316L stainless steel is modified as a consequence of the micro-plasma arc welding process.
2. Open circuit potential measurements show that both the non-welded and the micro-plasma arc welded alloys have a passive behaviour in phosphoric acid at the different temperatures studied.
3. Better passivation film properties are expected for the non-welded stainless steel since higher passivity ranges and lower passivation current densities are obtained for the non-welded stainless steel.
4. The corrosion rate of AISI 316L stainless steel increases owing to the galvanic effect. This is confirmed by the E_a values calculated from the Arrhenius plot.
5. The imposed potential measurements provide more active predicted coupled potentials and higher coupled current densities than those obtained using ZRA measurements. The galvanic potential values obtained by means of the ZRA technique are closer to the open circuit potential values of the uncoupled materials than to the predicted coupled potentials.
6. Results show that i_{coup} values increase with temperature. ZRA tests measured the highest i_G value at 60 ºC; however, the i_G values are very close to zero for all the temperatures studied. This is in agreement with the low (E_{corr_C} - E_{corr_A}) and i_{coup}/i_{corr} values obtained. The most positive E_{coup} and E_G values are obtained at the highest temperature studied (60 ºC).

7. This study reveals that micro-plasma arc welded AISI 316L stainless steels are appropriated working in the studied H_3PO_4 media from a corrosion point of view for all the temperatures analysed.

Acknowledgments

The authors would like to express their gratitude to the Spanish MAEC (PCI Mediterráneo C/8196/07, C/018046/08, D/023608/09) and to Asuncion Jaime for her translation assistance.

References

[1] A.I. Almarshad, D. Jamal, Electrochemical investigations of pitting corrosion behaviour of type UNS S31603 stainless steel in thiosulfate-chloride environment, J. Appl. Electrochem. 34 (2004) 67-70.

[2] J. Oñoro, Corrosion fatigue behaviour of 317LN austenitic stainless steel in phosphoric acid, Int. J. Pres. Ves. Pip. 86 (2009) 656-660.

[3] R.W.K. Honeycombe, H.K.D.H. Bhadeshia, Steels. Microstructure and properties, third ed., Butterworth Heinemann, Great Britain, 2006.

[4] M. Dadfar, M.H. Fathi, F. Karimzadeh, M.R. Dadfar, A. Saatchi, Effect of TIG welding on corrosion behaviour of 316L stainless steel, Mat. Lett. 61 (2007) 2343-2346.

[5] P. Becker, Phosphates and phosphoric acid. Raw materials, technology, and economics of the wet process, second ed., Marcel Dekker, New York, 1989.

[6] A. Guenbour, H. Iken, N. Kebkab, A. Bellaouchou, R. Boulif and A. Benbachir, Corrosion of graphite in industrial phosphoric acid, Appl. Surf. Sci. 252 (2006) 8710-8715.

[7] A.Y. Musa, A.A.H. Kadhum, A. Bakar-Mohamad, A. Razak-Daud, M. Sobri-Takriff, S. Kartom-Kamarudin and N. Muhamad, Stability of layer forming for corrosion inhibitor on mild steel surface under hydrodynamic conditions, Int. J. Electrochem. Sci. 4 (2009) 707-716.

[8] J. Niu, W. Guo, M. Guo and S. Lu, Plasma application in thermal processing of materials, Vacuum 65 (2002) 263-266.

[9] F. Javidrad and R. Rahmati, An integrated re-engineering plan for the manufacturing of aerospace components, Mater. Design 30 (2009) 1524-1532.

[10] F. Javidrad, H. Farghadani, A. Asgharzadeh, Microplasma arc welding of AISI 304 stainless steel for use in aerospace industries, J. Sci. Eng. 31 (2008) 67-77.

[11] F. Karimzadeh, A. Ebnonnasir and A. Foroughi, Artificial neural network modeling for evaluating of epitaxial growth of Ti6Al4V weldment, Mater. Sci. Eng. A 432 (2006) 184-190.

[12] F. Karimzadeh, M. Salehi, A. Saatchi, M. Meratian, Effect of microplasma arc welding, process parameters on grain growth and porosity distribution of thin sheet Ti6Al4V alloy weldment, Mater. Manuf. Process. 20 (2005) 205-219.

[13] P.R. Roberge, Handbook of Corrosion Engineering, first ed., McGraw-Hill, USA 1999.

[14] J.R. Kearns, D.A. Eden, M.R. Yaffe, J.V. Fahey, D.L. Reichert, D. C. Silverman, ASTM Standardization of Electrochemical Noise Measurement ASTM STP 1277, 1996.

[15] M. Benabdellah, B. Hammouti, Corrosion behaviour of steel in concentrated phosphoric acid solutions, Appl. Surf. Sci. 252 (2005) 1657-1661.

[16] A. Bellaouchou, A. Guenbour, A. Benbachir, Corrosion behaviour of stainless steel in phosphoric acid polluted by sulfide ions, Corrosion 49 (1993) 656-662.

[17] H. Iken, R. Basseguy, A. Guenbour, A. Benbachir, Classic and local analysis of corrosion behaviour of graphite and stainless steels in polluted phosphoric acid, Electrochim. Acta, 52 (2007) 2580-2587.

[18] S.C. Dexter and J.P. LaFontaine, Effect of natural marine biofilms on galvanic corrosion, Corrosion 54 (1998) 851-861.

[19] P. Bala Srinivasan and M.P. Satish Kumar, Microstructural and electrochemical characterization of a thin-section dissimilar stainless steel weld joint, Mater. Chem. Phys. 115 (2009) 179-184.

[20] D-Q. Zhang, J. Li, H. Goun-Joo and K. Yong-Lee, Corrosion properties of Nd:YAG laser–GMA hybrid welded AA6061 Al alloy and its microstructure, Corros. Sci. 51 (2009) 1399-1404.

[21] E. Mohammadi Zahrani, A. Saatchi and A. Alfantazi, Pitting of 316L stainless steel in flare piping of a petrochemical plant, Eng. Fail. Anal. 17 (2010) 810-817.

[22] M.P. Satish Kumar and P. Bala Srinivasan, Corrosion behaviour of a thin section martensitic stainless steel GTA weldment in chloride solutions, Mater. Lett. 62 (2008) 2887-2890.

[23] S. Ahila, S.Ramakrishna Iyer and V.M. Radhakrishnan, A comparative study of hot corrosion of welded and unwelded 2.25 Cr-1Mo steel, Mater. Lett. 16 (1993) 130-133.

[24] C. Lin, X. Li and C. Dong, Pitting and galvanic corrosion behaviour of stainless steel with weld in wet-dry environment containing Cl^-, J. Univ. Sci. Technol. Beijing 14 (2007) 517-522.

[25] M. Gojic, D. Marijan, M. Tudja and S. Kozuh, Passivation of welded AISI 316L stainless steel, RMZ Materials and Geoenvironment 55 (2008) 408-419.

[26] C.T. Kwok, S.L. Fong, F.T. Cheng and H.C. Man, Pitting and galvanic corrosion behaviour of laser-welded stainless steels, J. Mater. Process. Technol. 176 (2006) 168-178.

[27] D.J. Lee, K.H. Jung, J.H. Sung, Y.H. Kim, K.H. Lee, J.U. Park, Y.T. Shin, H.W. Lee, Pitting corrosion behaviour on crack property in AISI 304L weld metals with varying Cr/Ni equivalent ratio, Mater. Design 30 (2009) 3269-3273.

[28] C. Wagner, W. Traud, Zeitschrift Fur Elektrochemie Und Angewandte Physikalische Chemie. Elektrochem 44 (1938) 391-454.

[29] L. Jeffus, Welding. Principles and Applications, fifth ed., Thomson Delmar Learning, USA, 1997.

[30] G. F. Vander Voort, Metallography. Principles and practice, ASM International, second ed., USA, 1999.

[31] R. Sánchez-Tovar, M.T. Montañés, J. García-Antón, The effect of temperature on the galvanic corrosion of the copper/AISI 304 pair in LiBr solutions under hydrodynamic conditions, Corros. Sci. 52 (2010) 722-733.

[32] N. Perez, Electrochemistry and corrosion science, first ed., Kluwer Academic Publishers, USA, 2004.

[33] H.P. Hack, Evaluation of galvanic corrosion, Corrosion: Fundamentals, Testing and Protection, Vol 13A, ASM Handbook, ASM International, USA, 2003.

[34] L. Reclaru, R. Lerf, P.-Y. Eschler, A. Blatter and J.-M. Meyer, Pitting, crevice and galvanic corrosion of REX stainless-steel/CoCr orthopaedic implant material, Biomaterials 23 (2002) 3479-3485.

[35] F. Mansfeld, Z. Sun, C.H. Hsu and A. Nagiub, Concerning trend removal in electrochemical noise measurements, Corros. Sci. 43 (2001) 341-352.

[36] L. Reclaru, R. Lerf, P. -Y. Eschler and J.-M. Meyer, Corrosion behavior of a welded stainless-steel orthopedic implant, Biomaterials 22 (2001) 269-279.

[37] E. Blasco-Tamarit, A. Igual-Muñoz, J. García Antón and D. García-García, Comparison between open circuit and imposed potential measurements to evaluate the effect of temperature on galvanic corrosion of the pair alloy 31–welded alloy 31 in LiBr solutions, Corros. Sci. 50 (2008) 3590-3598.

[38] E. Blasco-Tamarit, A. Igual-Muñoz, J. García Antón and D. García-García, Corrosion behaviour and galvanic coupling of titanium and welded titanium in LiBr solutions, Corros. Sci. 49 (2007) 1000-1026.

[39] E. Blasco-Tamarit, A. Igual-Muñoz and J. García Antón, Galvanic corrosion of high alloyed austenitic stainless steel welds in LiBr systems, Corros. Sci. 49 (2007) 4452-4471.

[40] E. Blasco-Tamarit, A. Igual-Muñoz, J. García Antón and D. García-García, Effect of aqueous LiBr solutions on the corrosion resistance and galvanic corrosion of an austenitic stainless steel in its welded and non-welded condition, Corros. Sci. 48 (2006) 863-886.

[41] G. Conde y Santiago, Aceros inoxidables, refractarios y criogenicos, first ed., INTERCIENCIA, Madrid, 1971.

[42] T.Y. Kuo, H.T. Lee, Effects of filler metal composition on joining properties of alloy 690 weldments, Mater. Sci. Eng. A 338 (2002) 202-212.

[43] G.F. Vander Voort, H.M. James, Wrought stainless steels. ASM Handbook. Vol. 9. Metallography and Microstructures. ASM International, USA, 1985. pp. 279-296.

[44] M. Reffass, R. Sabot, M. Jeannin, C. Berziou, Ph. Refait, Effects of phosphate species on localised corrosion of steel in NaHCO3 + NaCl electrolytes, Electrochim. Acta 54 (2009) 4389-4396.

[45] E. Almeida, D. Pereira, M. O. Figueiredo, V. M. M. Lobo, M. Morcillo, The influence of the interfacial conditions on rust conversion by phosphoric acid, Corros. Sci. 39 (1997) 1561-1570.

[46] S.R. Moraes, D. Huerta-Vilca and A.J. Motheo, Corrosion protection of stainless steel by polyaniline electrosynthesized from phosphate buffer solutions, Prog. Org. Coat. 48 (2003) 28-33.

[47] ASTM G-5 Test method for making potentiostatic and potentiodynamic anodic polarization measurements, 2004.

[48] M.A. Rodríguez, R.M. Carranza and R.B. Rebak, Passivation and Depassivation of Alloy 22 in Acidic Chloride Solutions, J. Electrochem. Soc. 157 (2010) C1-C8.

[49] L.L. Shreir, R.A. Jarman, G.T. Burstein, Corrosion Volume I Metal/Environment Reactions, third ed., Butterworth-Heinemann, Great Britain, 1994.

[50] A. Guenbour, M.A. Hajji, E.M. Jallouli and A. Ben-Bachir, Study of corrosion–erosion behaviour of stainless alloys in industrial phosphoric acid medium, Appl. Surf. Sci. 253 (2006) 2362-2366.

[51] C. Lavos-Valereto, I. Costa and S. Wolynec, The electrochemical behavior of Ti–6Al–7Nb alloy with and without plasma-sprayed hydroxyapatite coating in Hank's solution, J. Biomed. Mater. Res. 63 (2002) 664-670.

[52] S. Luiz de Assis, S. Wolynec and I. Costa, Corrosion characterization of titanium alloys by electrochemical techniques, Electrochim. Acta 51 (2006) 1815-1819.

[53] M. Kaneko, H.S. Isaacs, Pitting of stainless steel in bromide, chloride and bromide/chloride solutions, Corros. Sci. 42 (2000) 67-78.

[54] A. Neville, T. Hodgkiess, An assessment of the corrosion behaviour of high-grade alloys in seawater at elevated temperature and under a high velocity impinging flow, Corros. Sci. 38 (1996) 927-956.

[55] G.T. Burstein, C. Liu, R.M. Souto, The effect of temperature on the nucleation of corrosion pits on titanium in Ringer's physiological solution, Biomaterials 26 (2005) 245-256.

[56] F.J. Botana, A. Aballe, M. Marcos, Ruido Electroquímico. Métodos de análisis, first ed., Septem Ediciones, Oviedo, 2002.

[57] E. Otero Huerta, Corrosión y degradación de materiales, first ed., Síntesis, Madrid, 1997.

[58] F. Mansfeld, J.V. Kendel, Laboratory studies of Galvanic corrosion of aluminium alloys, Galvanic and pitting Corrosion-Field and Laboratory Studies in: R Baboian, WD France, Jr, LC Roew and JF Rynewicz (Eds.), Galvanic and pitting corrosion-field and laboratory studies, ASTM STP 576, ASTM, Philadelphia, 1976, pp. 20-47.

[59] F.T. Cheng, K.H. Lo, H.C. Man, NiTi cladding on stainless steel by TIG surfacing process Part II. Corrosion behavior, Surf. Coat. Tech. 172 (2003) 316-321.

[60] A.J. Bard, L.R. Faulkner, Electrochemical methods. Fundamentals and Applications, second ed, John Wiley & Sons, Inc, USA, 2001.

[61] L.F. Garfias-Mesias, J.M. Sykes, Metastable pitting in 25 Cr duplex stainless steel, Corros. Sci. 41 (1999) 959-987.

[62] N.J. Laycock, Effects of Temperature and Thiosulfate on Chloride Pitting of Austenitic Stainless Steels, Corrosion 55 (1999) 590-595.

[63] A. Pardo, E. Otero, M.C. Merino, M.D. López, M.V. Utrilla, F. Moreno, Influence of pH and Chloride Concentration on the Pitting and Crevice Corrosion Behavior of High-Alloy Stainless Steels, Corrosion 56 (2000) 411-418.

[64] M.R. El Sherif, M.I. Khaled and A.B. Waheed, Effect of Zn and Pb as alloying elements on the electrochemical behavior of brass in NaCl solutions, Electrochim. Acta 49 (2004) 5139-5150.

[65] P.W. Atkins, Physical Chemistry, sixth ed, Oxford University Press, USA (1998).

TABLES

Table 1. Mean values of the corrosion current densities (i_{corr}) and corrosion potentials (E_{corr}) of non-welded (NW) and MPA welded (W) AISI 316L SS in 5.5 M H_3PO_4 solutions at *Re* = 1456 and at different temperatures.

Table 2. Mean values of the passivation current densities (i_p) and critical potentials (E_c) of non-welded (NW) and MPA welded (W) AISI 316L SS in 5.5 M H_3PO_4 solutions at *Re* = 1456 and at different temperatures.

Table 3. Mean values of the galvanic current densities and the galvanic potentials obtained during eight hours by means of the ZRA measurements of the non-welded/MPA welded AISI 316L SS pair in 5.5 M H_3PO_4 solutions at *Re* = 1456 and at different temperatures.

Table 4. Mean values of the coupled current densities and the potentials obtained by the application of the mixed potential theory of the non-welded/MPA welded AISI 316L SS pair in 5.5 M H_3PO_4 solutions at *Re* = 1456 and at different temperatures.

FIGURES

Figure 1. Scheme of the materials used, as well as the photographs of the different materials studied: non-welded AISI 316L SS and MPA welded AISI 316L SS.

Figure 2. Photographs of the inner surface of the tubes, a: Base SS (non-welded) b: MPA welded SS.

Figure 3. Schematic diagram of the physical arrangement of the electrodes in the test section to carry out polarization curves. AE: auxiliary electrode. RE: reference electrode. WE: working electrode.

Figure 4. Schematic diagram of the physical arrangement of the electrodes in the test section to carry out ZRA measurements. RE: reference electrode. NW: non-welded AISI 316L SS. W: MPA welded AISI 316L SS.

Figure 5. Microstructure of the non-welded AISI 316L SS (a) and the MPA welded SS corresponding to the HAZ (b) and to the weld bead (c) examined by LM and SEM.

Figure 6. Open circuit potential registers of the non-welded (a) and MPA welded (b) AISI 316L SS in 5.5 M H_3PO_4 solutions at a Reynolds number of 1456 and different temperatures.

Figure 7. Cyclic polarization curves of the non-welded (a) and MPA welded (b) AISI 316L SS in 5.5 M H_3PO_4 solutions at a Reynolds number of 1456 and different temperatures. Vertical lines indicate the mean values of the *OCP*.

Figure 8. Passivity ranges of the non-welded (a) and MPA welded (b) AISI 316L SS in 5.5 M H_3PO_4 solutions at a Reynolds number of 1456 and at different temperatures.

Figure 9. Galvanic current density (a) and potential profiles (b) of the non-welded/MPA welded AISI 316L SS pair at a *Re* of 1456 at the different temperatures analysed in 5.5 M H_3PO_4 solutions.

Figure 10. Comparison between the results obtained by the mixed potential theory (i_{coup} and E_{coup}) and the ZRA technique (■) for the non-welded/MPA welded AISI 316L stainless steel galvanic pair at a *Re* of 1456 at the different temperatures analysed in 5.5 M H_3PO_4 solutions.

Figure 11. Dependence of the mean values of the corrosion current densities of the non-welded AISI 316L SS and coupled current densities of the pair (obtained from the mixed potential theory, MPT) on the temperature according to Arrhenius plot.

Table 1

	25 ºC		40 ºC		60 ºC	
	NW	W	NW	W	NW	W
$i_{corr} \pm \sigma$ (μA/cm^2)	4.92 ± 0.10	4.51 ± 0.09	6.41 ± 0.12	2.10 ± 0.07	10.18 ± 0.19	2.02 ± 0.04
$E_{corr} \pm \sigma$ ($mV_{Ag/AgCl}$)	-282 ± 1	-192 ± 8	-251 ± 7	-85 ± 10	-250 ± 4	-118 ± 4

Table 2

	25 ºC		40 ºC		60 ºC	
	NW	W	NW	W	NW	W
$i_p \pm \sigma$ (μA/cm^2)	5.68 ± 0.45	19.15 ± 2.07	9.38 ± 1.02	11.10 ± 1.34	9.09 ± 1.45	9.24 ± 1.95
$E_c \pm \sigma$ (mV$_{Ag/AgCl}$)	1158 ± 14	1149 ± 19	1124 ± 1	1098 ± 11	1083 ± 9	1074 ± 10

Table 3

	25 ºC		40 ºC		60 ºC	
Time (h)	$i_G \pm \sigma$ ($\mu A/cm^2$)	$E_G \pm \sigma$ ($mV_{Ag/AgCl}$)	$i_G \pm \sigma$ ($\mu A/cm^2$)	$E_G \pm \sigma$ ($mV_{Ag/AgCl}$)	$i_G \pm \sigma$ ($\mu A/cm^2$)	$E_G \pm \sigma$ ($mV_{Ag/AgCl}$)
1	-0.46 ± 0.12	-132 ± 17	-0.63 ± 0.11	-121 ± 5	-1.21 ± 0.15	-78 ± 15
2	-0.34 ± 0.01	-97 ± 5	-0.21 ± 0.07	-32 ± 7	0.36 ± 0.06	122 ± 11
3	-0.25 ± 0.07	-55 ± 5	-0.01 ± 0.00	65 ± 10	0.22 ± 0.01	211 ± 28
4	0.00 ± 0.00	77 ± 12	0.02 ± 0.00	120 ± 20	0.13 ± 0.01	232 ± 26
5	0.00 ± 0.00	128 ± 11	0.03 ± 0.00	148 ± 15	0.09 ±0.02	247 ± 29
6	-0.02 ± 0.00	149 ± 6	0.03 ± 0.00	171 ± 15	0.07 ± 0.02	243 ± 19
7	-0.02 ± 0.00	148 ± 4	0.03 ± 0.00	192 ± 21	0.07 ± 0.01	261 ± 28
8	-0.03 ± 0.00	152 ± 2	0.03 ± 0.00	202 ± 17	0.04 ± 0.01	262 ± 24

Table 4

	25 ºC	**40 ºC**	**60 ºC**
$i_{coup} \pm \sigma$ **(μA/cm²)**	5.92 ± 0.15	7.04 ± 0.36	11.69 ± 0.35
$E_{coup} \pm \sigma$ **($mV_{Ag/AgCl}$)**	-218 ± 9	-203 ± 12	-195 ± 5
$E_{corr\_C} - E_{corr\_A}$ **(mV)**	90	165	131
i_{coup}/i_{corr}	1.20	1.10	1.15

Figure 1

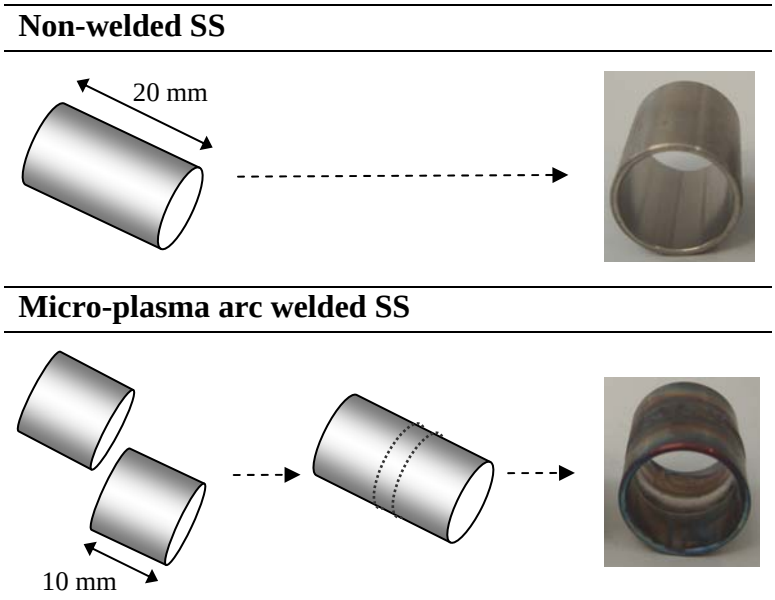

Figure 2

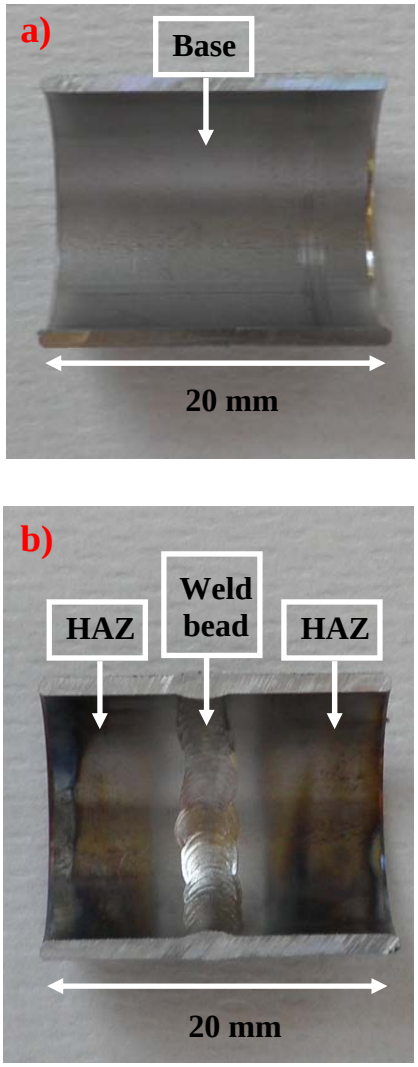

Figure 3

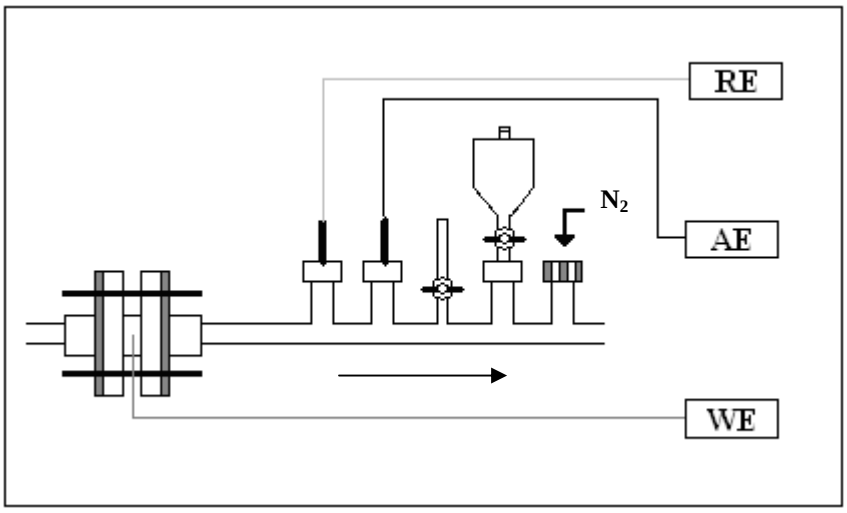

Figure 4

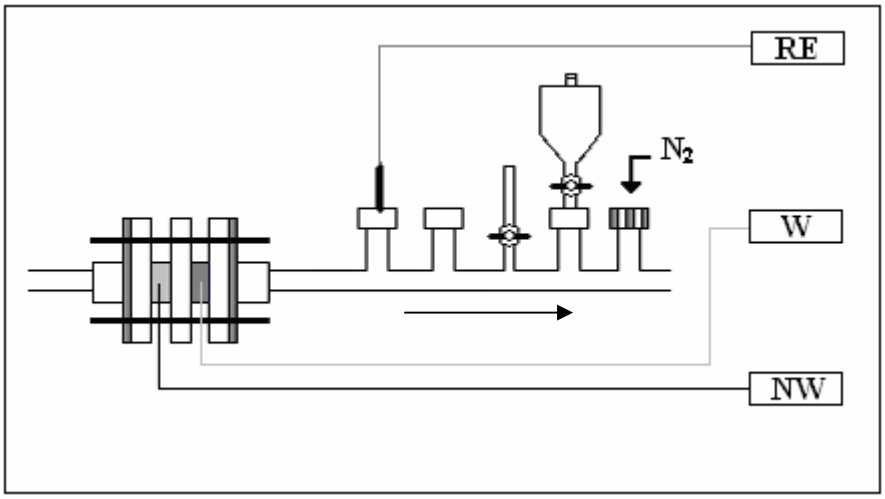

Figure 5

LM **SEM**

a. NON WELDED SS

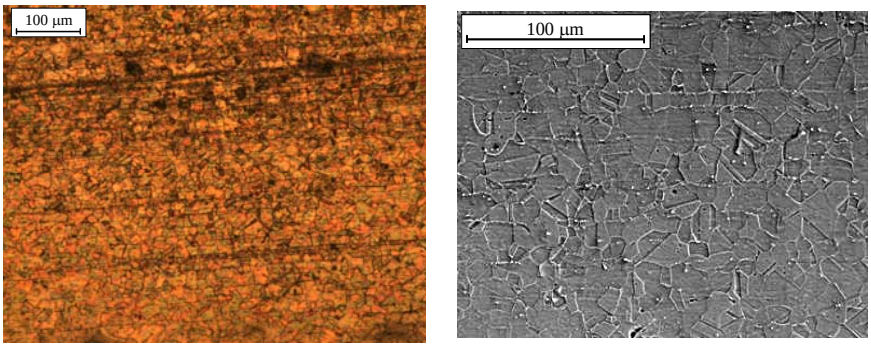

b. MPA WELDED SS: HAZ

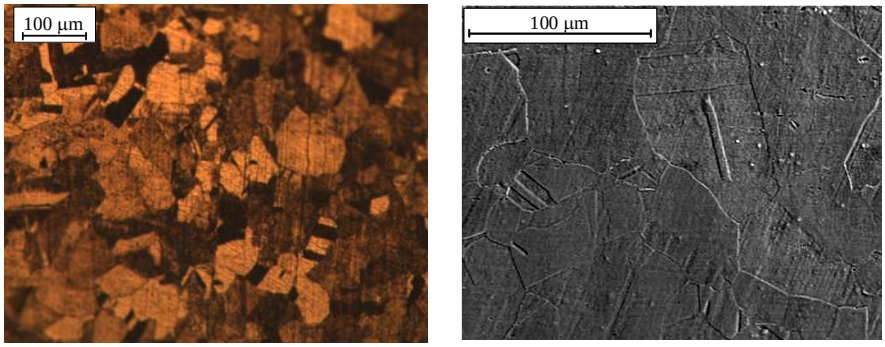

c. MPA WELDED SS: Weld bead

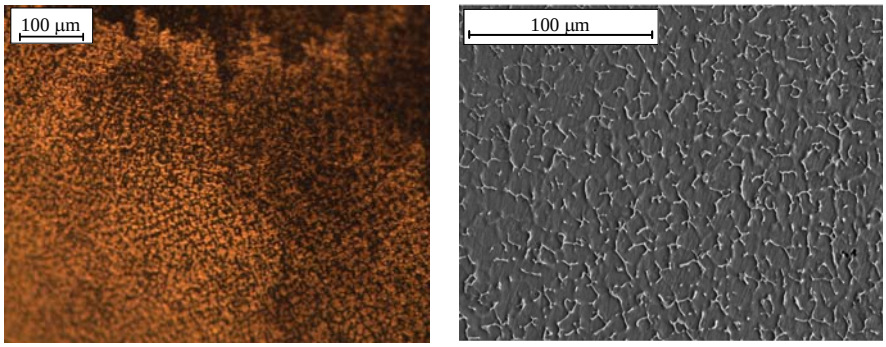

Figure 6

a. Non-welded AISI 316L SS

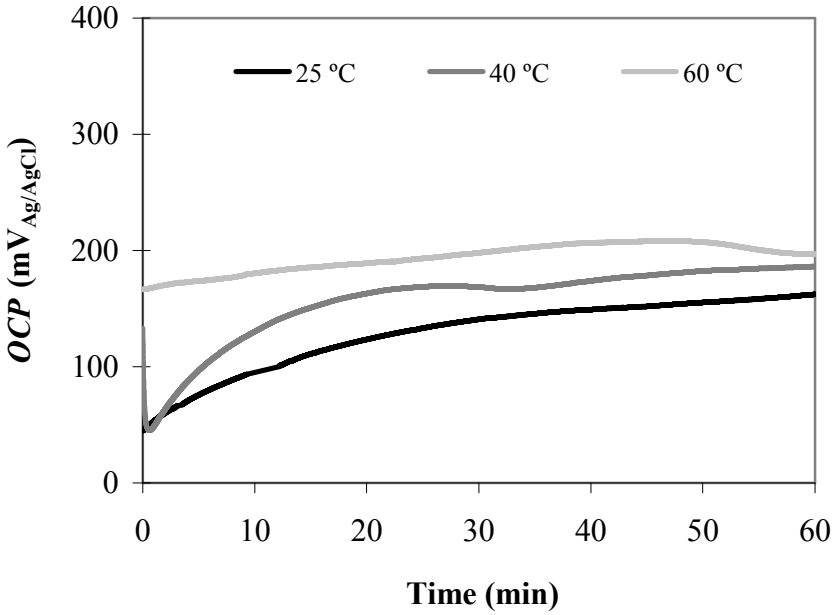

b. Welded AISI 316L SS

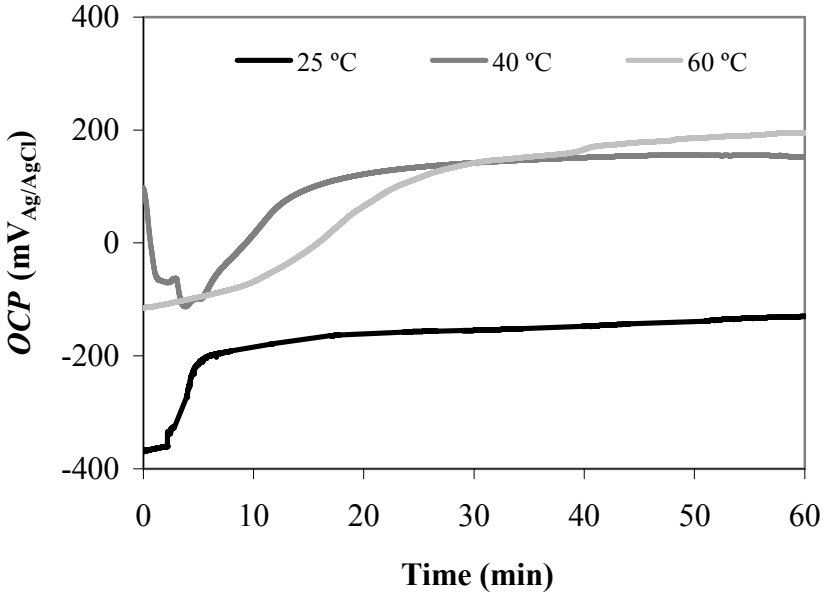

Figure 7

a. Non-welded AISI 316L SS

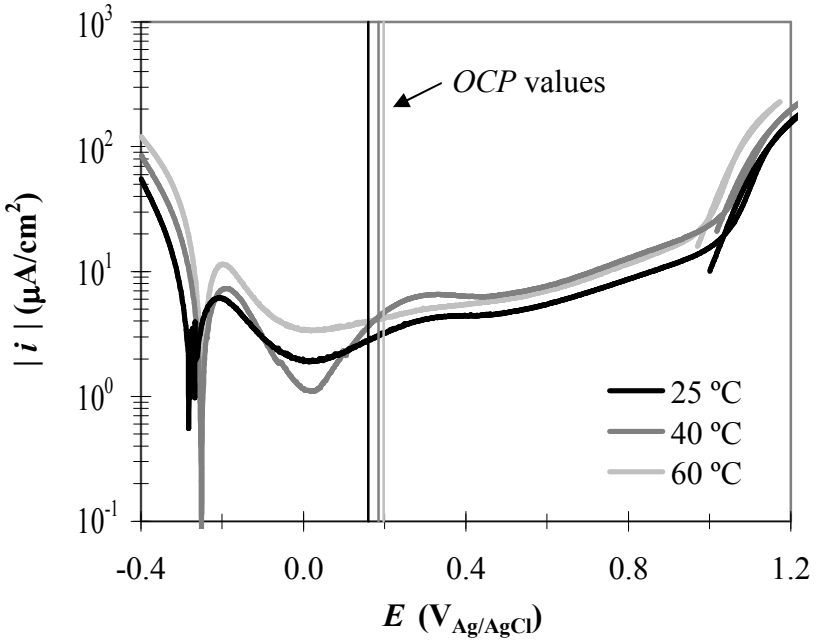

b. Welded AISI 316L SS

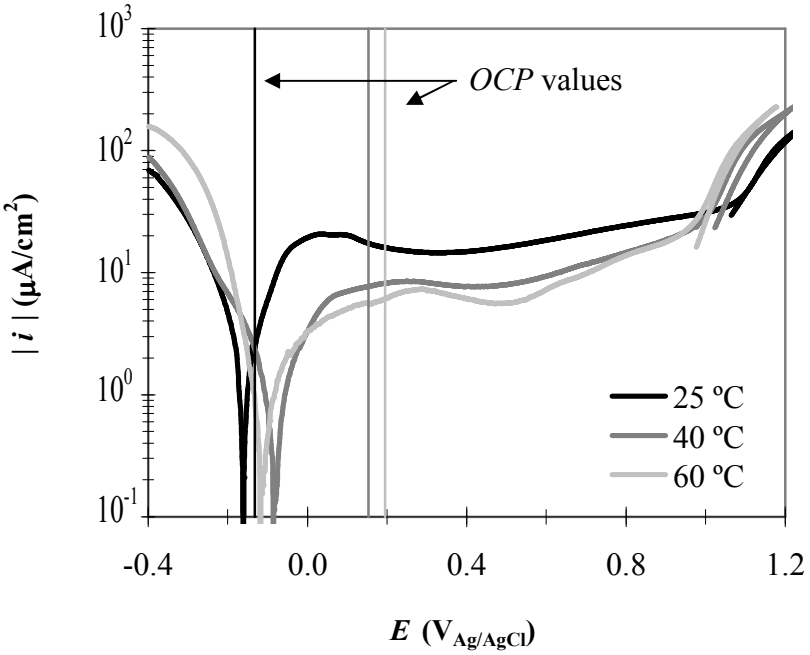

Figure 8

a. Non-welded AISI 316L SS

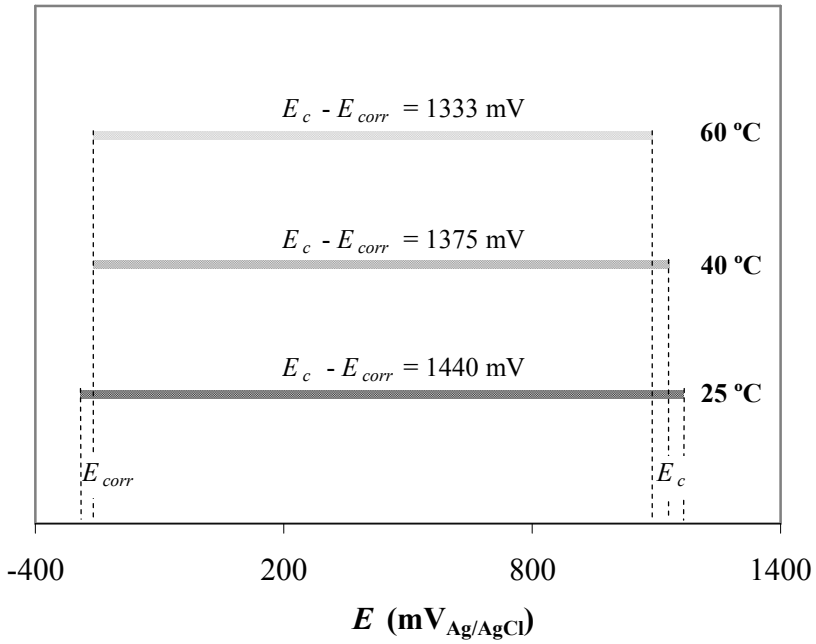

b. Welded AISI 316L SS

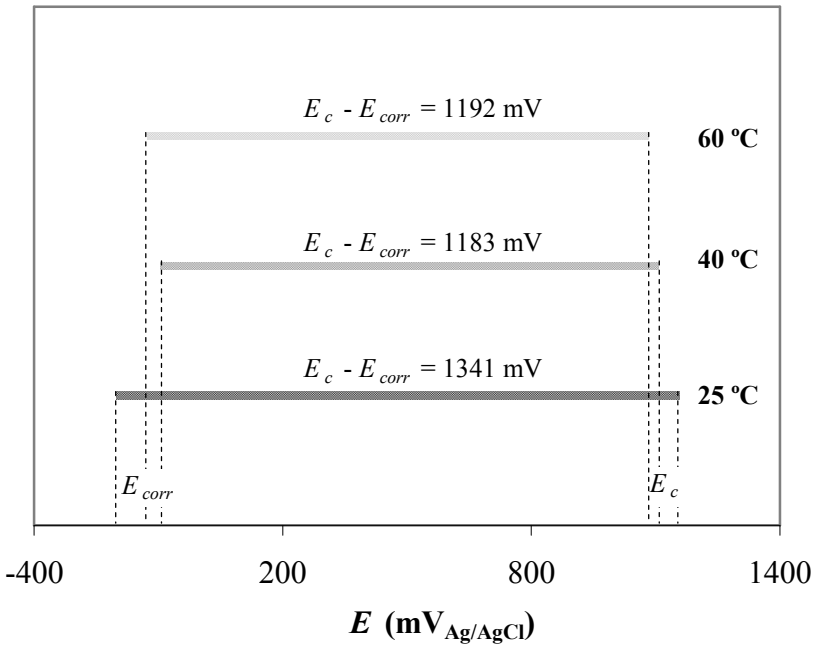

Figure 9

a.

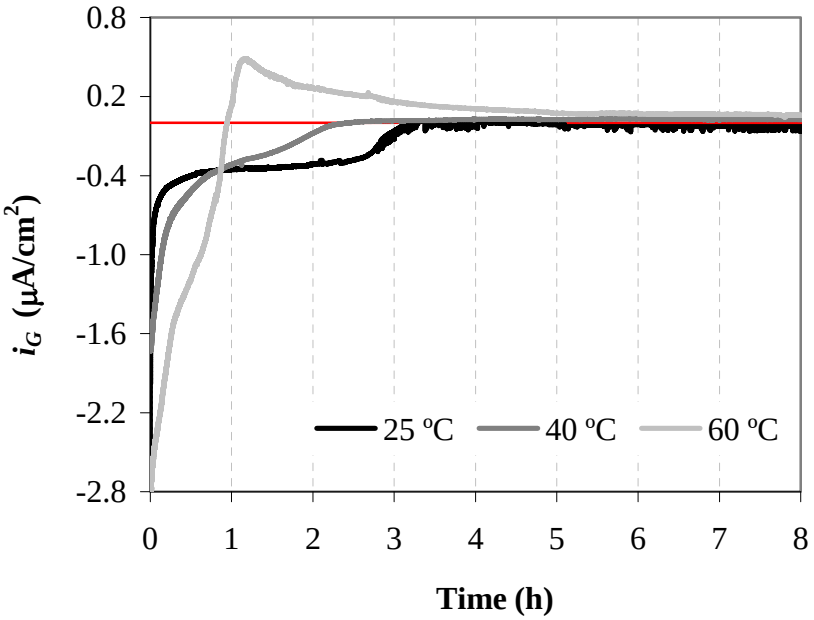
0.8
0.2
-0.4
-1.0
-1.6
-2.2
-2.8
i_G (µA/cm^2)
25 ºC
40 ºC
60 ºC
0
1
2
3
4
5
6
7
8
Time (h)

b.

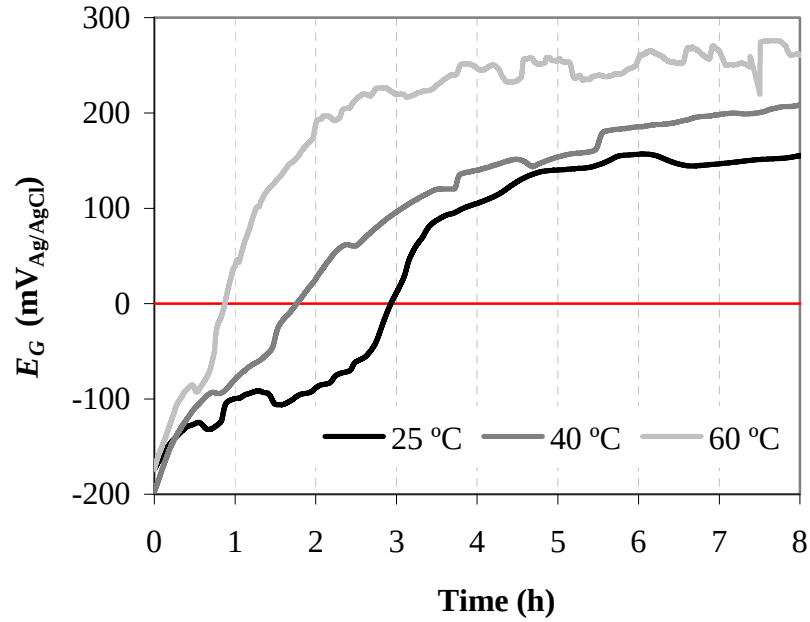
300
200
100
0
-100
-200
E_G (mV$_{Ag/AgCl}$)
25 ºC
40 ºC
60 ºC
0
1
2
3
4
5
6
7
8
Time (h)

Figure 10

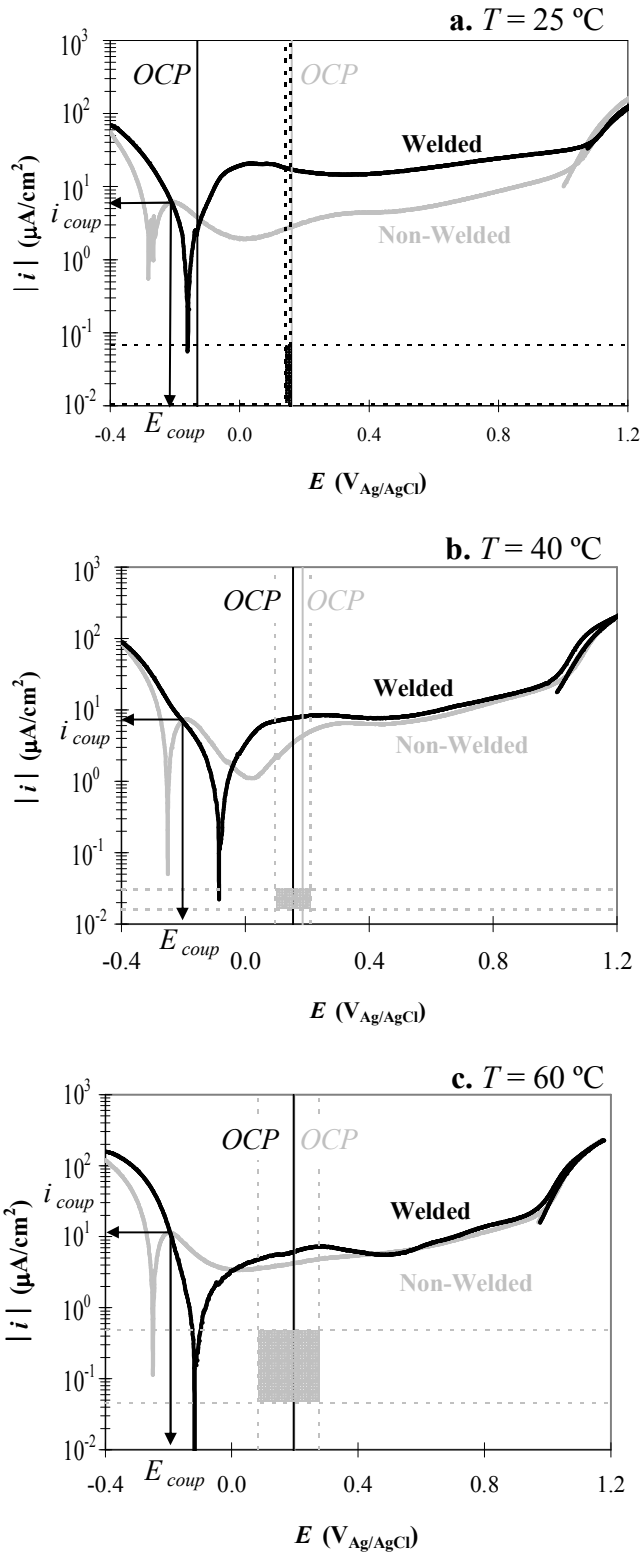
a. T = 25 ºC
OCP
OCP
Welded
Non-Welded
i coup
E coup
| i | (µA/cm²)
E (V Ag/AgCl)
b. T = 40 ºC
OCP
OCP
Welded
Non-Welded
i coup
E coup
| i | (µA/cm²)
E (V Ag/AgCl)
c. T = 60 ºC
OCP
OCP
Welded
Non-Welded
i coup
E coup
| i | (µA/cm²)
E (V Ag/AgCl)

Figure 11

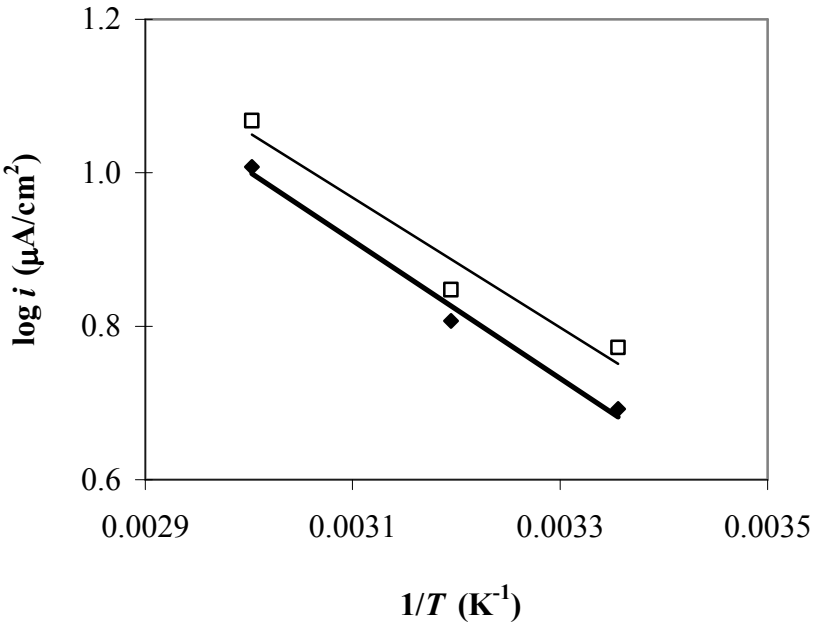

□ MPT log i_{coup} = 3.60 - 847.68 (1/T); R^2 = 0.950

◆ non-welded log i_{corr} = 3.70 - 900.16 (1/T); R^2 = 0.989